Coherent two-dimensional Raman scattering: Frequency-domain measurement of the intra- and intermolecular vibrational interactions

Minhaeng Cho,[a] Ko Okumura, and Yoshitaka Tanimura
Division of Theoretical Studies, Institute for Molecular Science, Myodaiji, Okazaki, Aichi 444, Japan

(Received 25 August 1997; accepted 16 October 1997)

A new experiment of frequency-domain coherent two-dimensional Raman scattering is theoretically proposed. By using three fields whose wave vectors and frequencies are independently controlled, one can measure the nonlinear Raman responses in either gas or condensed phases. The connection to the time-domain femtosecond two-dimensional Raman spectroscopy is completely established. By considering several limiting cases in detail, it is found that from the coherent 2D Raman scattering spectrum one can obtain quantitative information on the anharmonicity, anharmonic mode coupling, and polarizability coupling. © *1998 American Institute of Physics.*
[S0021-9606(98)01504-9]

I. INTRODUCTION

Vibrational spectroscopies such as infrared absorption and Raman scattering have been used in a wide variety of scientific studies. Because of the dramatic advent of laser spectroscopic techniques, coherent Raman scattering has been playing a crucial role in studying dynamics of intra- and intermolecular vibrational modes in either gas or condensed phases.[1–3] In the last decade, by using the subpicosecond laser pulses, the time-domain measurement of the Raman response of the liquid, such as optical Kerr effect (OKE)[4–9] or impulsive stimulated Raman scattering (ISRS),[10] has been carried out and provided information on the ultrafast dynamical responses from a variety of liquids and solutions. These methods are directly related to the frequency-domain coherent Raman or spontaneous Raman scattering processes based on the quantum fluctuation–dissipation theorem as discussed by Cho *et al.*[6] The outcome of these experiments provides vital information on the time scales of the liquid dynamics, which in turn can be used in understanding other types of nonlinear spectroscopic phenomena[11,12] as well as chemical reactions in condensed phases such as electron transfer.[13]

Recently, Tanimura and Mukamel suggested a new experimental method measuring the two-dimensional Raman response of liquids.[14] The essence of this method is that, by using two pairs of off-resonant femtosecond pulses followed by the final probe pulse and by controlling the two delay times, it is possible to probe the fifth-order time-domain Raman response. Subsequently Tominaga and Yoshihara,[15] Fleming and co-workers,[16] and Steffen and Duppen[17] carried out this experiment and found rich dynamics that could not be revealed by the third-order Raman response. Using Feynman diagrams, Okumura and Tanimura[18] investigated the role of anharmonicity and inhomogeneous broadening of inter- and intramolecular vibrations in time-domain 2D Raman experiments. Recently, Saito and Ohmine calculated time-domain 2D Raman signals for CS_2 and H_2O liquids based on the normal mode analysis and found that 2D Raman signals are very sensitive to the dynamics of molecules and mode coupling and can be used to extract rich information from the simulation studies.[19]

As mentioned above, the third-order Raman response has been measured by equivalent techniques in frequency-domain as well as in time-domain. In contrast, even though the time-domain 2D Raman scattering measurement utilizing femtosecond pulses have been already suggested and studied experimentally and also the direct 2D Fourier transform spectra were discussed,[16(b),16(c),18(c)] the corresponding 2D Raman scattering method in the *frequency-domain* has not been discussed yet. Here the theoretical description of the coherent 2D Raman scattering (COTRAS) is presented. It turns out that one needs at least three fields, whose frequencies and wave vectors are $(\omega_1,\mathbf{k}_1)$, $(\omega_2,\mathbf{k}_2)$, and $(\omega_3,\mathbf{k}_3)$ (see Fig. 1). By tuning the two difference frequencies among the three different fields, $\Omega_1 \equiv \omega_1 - \omega_2$ and $\Omega_2 \equiv \omega_1 - \omega_3$, one can map the inter- and intramolecular vibrational dynamics onto the two-dimensional (Ω_1,Ω_2)-frequency space. Thus it becomes possible to get a crucial information on the anharmonicity, liquid inhomogeneity, mode coupling effects, etc., by using this novel experimental technique.

In Sec. II, the theoretical description of COTRAS is presented. The COTRAS spectra for several limiting cases are discussed with numerical calculations in Sec. III. A summary is given in Sec. IV.

II. COHERENT 2D RAMAN SCATTERING (COTRAS)

By using the semiclassical description of the radiation-matter interaction, the total Hamiltonian is assumed to be

$$H = H_0 - VE(\mathbf{r},t), \tag{1}$$

where H_0 denotes the Hamiltonian without the external field, and V is the electric dipole operator. In order to describe the COTRAS process, it is necessary to have at least three fields so that the total external electric field can be written as

[a]Permanent address: Department of Chemistry, Korea University, Seoul 136-701, Korea.

 © 1998 American Institute of Physics

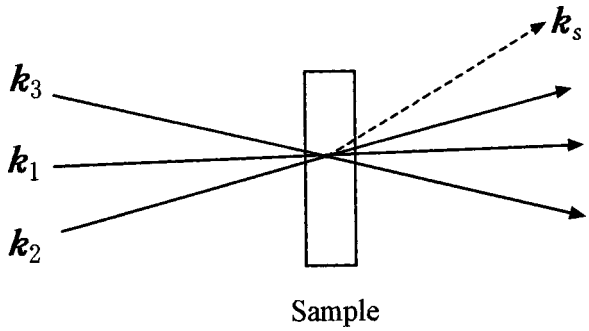

FIG. 1. Three off-resonant electric fields propagate with wave vectors, $\mathbf{k}_1$, $\mathbf{k}_2$, and $\mathbf{k}_3$, and frequencies ω_1, ω_2, and ω_3. From the phase matching condition, the coherent 2D Raman scattering field propagates with the wave vector $\mathbf{k}_s=3\mathbf{k}_1-\mathbf{k}_2-\mathbf{k}_3$ and the frequency $\omega_s=3\omega_1-\omega_2-\omega_3$.

$$E(\mathbf{r},t)=\sum_{j=1}^{3} E_j \exp(i\mathbf{k}_j\cdot\mathbf{r}-i\omega_j t)+\text{c.c.}, \tag{2}$$

where E_j denotes the electric field amplitude. Here, the three frequencies, ω_j $(j=1,2,3)$, are controlled experimentally. Since we are interested in the frequency-domain experiment, these fields are continuous waves. In case of coherent Raman scattering, the polarization, which acts as a source in the Maxwell equation for generated signal field, is created by the third-order radiation-matter interaction, whereas COTRAS is associated with the fifth-order process. Since we use off-resonant electric fields, by eliminating a Feynman vertex it is possible to describe the radiation–matter interaction with the effective Hamiltonian,[20]

$$H=H_g-\alpha(\mathbf{Q})E^2(\mathbf{r},t), \tag{3}$$

where H_g denotes the nuclear Hamiltonian of the electronic ground state and $\alpha(\mathbf{Q})$ represents the collective polarizability of the optical sample. If one considers the off-resonant optical response from a dilute gas, the collective polarizability $\alpha(\mathbf{Q})$ is likely to be similar to the individual molecular quantity. However, in a liquid, interaction-induced contribution to the collective polarizability should be taken into account.[21] Now inserting Eq. (2) into $E^2(\mathbf{r},t)$ returns 36 terms to be considered. However, only a few of them are relevant to the COTRAS process, as will be shown below. By considering the second term in Eq. (3) as a perturbative Hamiltonian and using conventional time-dependent perturbation theory, one can easily obtain the fifth-order polarization, which in turn can be expressed in terms of the nonlinear response function [see Eq. (8) below]. In order to select the relevant contributions from the general result, it is useful to first discuss the radiation–matter interaction processes corresponding to COTRAS.

In Fig. 2, the eigenstates of a given vibrational degree of freedom are shown. We find that three states are enough to discuss COTRAS. We consider the case where the system is initially in the state $|a\rangle$. The two interactions with $(\omega_1,\mathbf{k}_1)$ and $(\omega_2,\mathbf{k}_2)$ fields create a vibrational coherence state between $|a\rangle$ and $|b\rangle$, and the second two interactions with $(\omega_1,\mathbf{k}_1)$ and $(\omega_3,\mathbf{k}_3)$ fields create the second vibrational coherence state between $|b\rangle$ and $|c\rangle$. These consecutive processes can be interpreted as follows. The first two interactions create the spatial grating with frequency $\omega_1-\omega_2$, and the second two interactions create the second spatial grating with frequency $\omega_1-\omega_3$. Then the final interaction with $(\omega_1,\mathbf{k}_1)$ field creates the coherence state between a virtual state and $|a\rangle$, which produces the polarization generating the COTRAS signal field. This last process can be understood as a scattering of the $(\omega_1,\mathbf{k}_1)$ field by the two spatial gratings. Of course, in the frequency-domain experiment, there is no time-ordering as prescribed above. Therefore, all possible permutations should be taken into account. Because of the phase-matching condition for COTRAS, the wave vector of the scattering field should be $\mathbf{k}_s=3\mathbf{k}_1-\mathbf{k}_2-\mathbf{k}_3$ and the field frequency is $\omega_s=3\omega_1-\omega_2-\omega_3$.

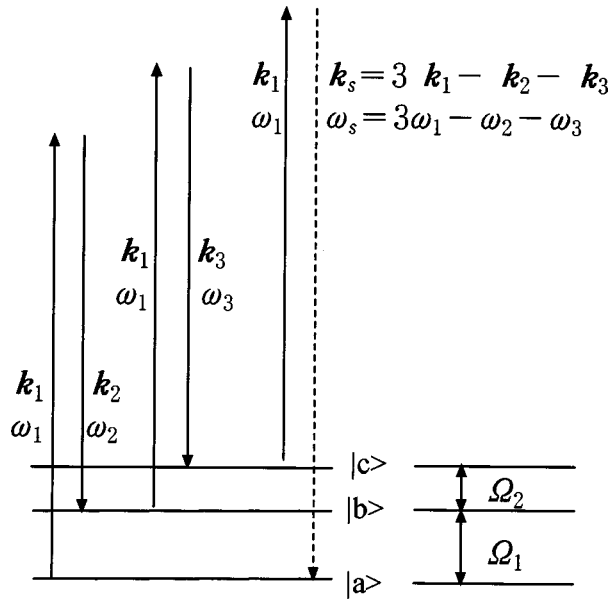

FIG. 2. Molecular energy level diagram for the COTRAS process.

The fifth-order polarization can be in general written in terms of the nonlinear response function,

$$P^{(5)}(\mathbf{r},t)=\int_0^\infty d\tau_1\cdots\int_0^\infty d\tau_5\, R^{(5)}(\tau_1,\ldots,\tau_5) \times\prod_{j=1}^{5} E\left(t-\sum_{k=j}^{5}\tau_k\right). \tag{4}$$

Inserting Eq. (2) produces 6^5 terms, but we only focus on the specific combination whose $\mathbf{r}$ and t dependences are given as

$$P^{(5)}(\mathbf{r},t)=E_1^3E_2^*E_3^*\exp\{i\mathbf{k}_s\cdot\mathbf{r}-i\omega_s t\}P^{(5)}_{\mathbf{k}_s}. \tag{5}$$

Here, the corresponding Fourier amplitude $P^{(5)}_{\mathbf{k}_s}$ carries the crucial information on the nonlinear Raman response from the optical sample, and we find that $P^{(5)}_{\mathbf{k}_s}$ is given by

$$P^{(5)}_{\mathbf{k}_s}=\widetilde{R}^{(5)}(\Omega_1,\Omega_1+\Omega_2)+\widetilde{R}^{(5)}(\Omega_2,\Omega_1+\Omega_2) \tag{6}$$

where Ω_1 and Ω_2 are the two difference frequencies among the three fields. The Fourier–Laplace transform of the fifth-order Raman response function is defined as

$$\widetilde{R}^{(5)}(\omega_\alpha,\omega_\beta)\equiv\int_0^\infty d\tau_1\int_0^\infty d\tau_2\, R^{(5)}(\tau_1,\tau_2)\times\exp(i\omega_\alpha\tau_1+i\omega_\beta\tau_2), \tag{7}$$

where

$$R^{(5)}(\tau_1,\tau_2)\equiv-\frac{1}{\hbar^2}\langle[[\alpha(\tau_1+\tau_2),\alpha(\tau_1)],\alpha(0)]\rangle. \tag{8}$$

In Eq. (8) $\alpha(t)(\equiv\exp(iH_gt/\hbar)\alpha\exp(-iH_gt/\hbar))$ is the polarizability operator in the Heisenberg picture at time t and these operators are propagated on the ground state potential energy surface. Thus the time-domain measurement of the response function, Eq. (8), can be directly related to the frequency-domain COTRAS via Eqs. (6) and (7). The COTRAS signal is proportional to the absolute square of the corresponding polarization,

$$S_{\mathrm{COTRAS}}(\Omega_1,\Omega_2)\propto|\widetilde{R}^{(5)}(\Omega_1,\Omega_1+\Omega_2)+\widetilde{R}^{(5)}(\Omega_2,\Omega_1+\Omega_2)|^2. \tag{9}$$

Note that the COTRAS spectrum is diagonally symmetric. This is because there is no time ordering of interactions with ω_2 and ω_3. Equation (9) is the principle result in this paper.

Since COTRAS is specifically designed to probe the two vibrational coherence states, vibrational resonance occur when the two difference frequencies, $\Omega_1\equiv\omega_1-\omega_2$ and $\Omega_2\equiv\omega_1-\omega_3$, are identical to the frequency gaps between any two vibrational states in the electronic ground state. Therefore the resonance conditions are

$$(\Omega_1=\omega_{ba}\ \text{ and }\ \Omega_2=\omega_{cb})\ \text{ or }\ (\Omega_1=\omega_{cb}\ \text{ and }\ \Omega_2=\omega_{ba}). \tag{10}$$

Depending on the signs of the two frequencies, Ω_1 and Ω_2, one may probe the deexcitation–deexcitation (D-D), excitation–excitation (E-E), deexcitation–excitation (D-E), and excitation–deexcitation (E-D) regions of the vibrational coherences, that correspond to the four frequency regions, ($\Omega_1<0$ and $\Omega_2<0$), ($\Omega_1\geqslant0$ and $\Omega_2\geqslant0$), ($\Omega_1<0$ and $\Omega_2\geqslant0$), and ($\Omega_1\geqslant0$ and $\Omega_2<0$), respectively.

Since we have two degrees of freedom of controlling frequencies, new features that could not be resolved in the third-order Raman scattering can be detected by this two-dimensional measurement. Although polarizability coupling and anharmonic effects were discussed in the context of the direct Fourier–Laplace transform of the time-domain nonlinear Raman response function,[16(b),16(c),18(c)] the arguments presented in the following section could provide a consistent and systematic way of analysing both the newly proposed frequency-domain experiment, COTRAS, and the direct Fourier–Laplace transform of the femtosecond 2D Raman measurement.

In order to specifically discuss the characteristic aspects of COTRAS in comparison to the lower-order Raman response, one should introduce models for the vibrational polarizability needed in Eq. (8).

III. NONLINEAR RAMAN RESPONSE FUNCTIONS AND COTRAS SPECTRA FOR MODEL SYSTEMS

In the following, we first consider the case when the vibrational degrees of freedom are harmonic and calculate the corresponding nonlinear Raman response function, and then we extend it to anharmonic cases. The nonlinear response function in Eq. (8) contains the collective polarizability operator, and one can in general expand this in terms of the nuclear degrees of freedom. Hereafter, several limiting cases are considered in detail.

A. A single damped harmonic oscillator

For the sake of simplicity, we first consider only one effective vibrational degree of freedom, whose coordinate is denoted as Q. Then one can express the polarizability as

$$\alpha=\alpha_0+\alpha_1Q+1/2\alpha_2Q^2+\cdots, \tag{11}$$

where

$$\alpha_1\equiv\left.\frac{\partial\alpha}{\partial Q}\right|_0,$$

$$\alpha_2\equiv\left.\frac{\partial^2\alpha}{\partial Q^2}\right|_0.$$

Usually by taking the first expansion term, that is linearly proportional to the vibrational coordinate, one can describe the third-order Raman response function. However, in the case of the fifth-order nonlinear Raman response, if only the first-order expansion term α_1Q is included, the trace in Eq. (8) becomes zero if the system is harmonic—note that the trace of the odd-power-coordinate terms, e.g., Q^3, over the canonical equilibrium density operator of the harmonic oscillator system vanishes. Therefore, at least one of the polarizability operators in the definition of the nonlinear Raman response function should contain a term that is proportional to α_2Q^2. Then the lowest-order contribution to $R^{(5)}(\tau_1,\tau_2)$ contains three-time correlation functions such as

$$-\frac{\alpha_1^2\alpha_2}{\hbar^2}\langle[[Q^2(\tau_1+\tau_2),Q(\tau_1)],Q(0)]\rangle, \tag{12a}$$

$$-\frac{\alpha_1^2\alpha_2}{\hbar^2}\langle[[Q(\tau_1+\tau_2),Q^2(\tau_1)],Q(0)]\rangle, \tag{12b}$$

$$-\frac{\alpha_1^2\alpha_2}{\hbar^2}\langle[[Q(\tau_1+\tau_2),Q(\tau_1)],Q^2(0)]\rangle. \tag{12c}$$

These terms can be understood by using the energy level scheme shown in Figs. 3(a), 3(b), and 3(c), respectively. Reading from right to left, we can interpret Eq. (12a) as a consecutive process, i.e., (i) one quantum excitation at time 0, (ii) one quantum excitation at $t=\tau_1$, and (iii) two quan-

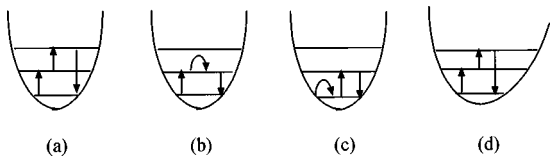

FIG. 3. Three consecutive processes associated with the three terms in Eqs. (12). (d) is the case of the anharmonic oscillator (see the context for detail).

tum deexcitation at $t=\tau_1+\tau_2$. Here, it should be mentioned that, because of the two commutators, Eq. (12a) contains four terms, e.g.,

$$-\frac{\alpha_1^2\alpha_2}{\hbar^2}\langle Q^2(\tau_1+\tau_2)Q(\tau_1)Q(0)\rangle,$$

$$\frac{\alpha_1^2\alpha_2}{\hbar^2}\langle Q(\tau_1)Q^2(\tau_1+\tau_2)Q(0)\rangle,$$

$$-\frac{\alpha_1^2\alpha_2}{\hbar^2}\langle Q(0)Q^2(\tau_1+\tau_2)Q(\tau_1)\rangle,$$

$$-\frac{\alpha_1^2\alpha_2}{\hbar^2}\langle Q(0)Q(\tau_1)Q^2(\tau_1+\tau_2)\rangle.$$

Only the first term in the above list, when reading from the right to left, can be interpreted as above. However, for the sake of convenience, throughout this paper, we shall interpret contributions like Eqs. (12) as discussed above in terms of a sequential excitation–deexcitation processes.

Although other excitation–deexcitation processes associated with Eq. (12a) are also possible, only the scheme shown in Fig. 3(a) contributes to the spectrum in the E-E region. Furthermore this contribution appears on the diagonal line ($\Omega_1=\Omega_2$) of the COTRAS spectrum at $\Omega_1=\omega_0$ and $\Omega_2=\omega_0$. Next we consider Eq. (12b), which can be interpreted as (i) one quantum excitation at time 0, (ii) simultaneous excitation and deexcitation at $t=\tau_1$, and (iii) one quantum deexcitation at $t=\tau_1+\tau_2$ [see Fig. 3(b)]. Consequently, the difference frequencies should be either ($\Omega_1=\omega_0$ and $\Omega_2=0$) or ($\Omega_1=0$ and $\Omega_2=\omega_0$), so that this contribution will show up as peaks on the Ω_1 and Ω_2 axes. Likewise, the contribution represented by Eq. (12c) also produces peaks on the Ω_1 and Ω_2 axes [see Fig. 3(c)]. Consequently one can find three distinctive peaks in the E-E region.

In this simple case, the nonlinear Raman response function can be analytically obtained as[14]

$$R^{(5)}(\tau_1,\tau_2)=\frac{4}{\hbar^2}\alpha_1^2\alpha_2[G(\tau_1)+G(\tau_1+\tau_2)]G(\tau_2). \tag{13}$$

$G(t)$ denotes the linear response function of the main oscillator Q, and is defined as

$$G(t)\equiv\int d\omega\, J(\omega)\sin(\omega t). \tag{14}$$

Here, the spectral density, $J(\omega)$, is related to the frequency distribution of the dissipation kernel of the harmonic mode in question. Depending on the model for the dynamics of the main oscillator, various functional forms for the spectral density are available. Here, for the sake of clarity, a few remarks are given for how to model the vibrational dephasing with Eq. (14). When $J(\omega)$ is sharply peaked at a given frequency ω_0, the main oscillator behaves almost like an underdamped oscillator so that the linear response function is proportional to $\sin\omega_0 t$. In case of the gas phase, this underdamped limit with a small dephasing constant can be used. On the other hand, if $J(\omega)$ has a broad feature around the main oscillator frequency ω_0, this vibrational mode behaves like a damped harmonic oscillator. In case of the simple Brownian oscillator model with the white noise approximation to the damping kernel, the linear response function is simply given as

$$G(t)\propto\exp(-\gamma t/2)\sin\Omega t, \tag{15}$$

where γ denotes the damping constant, and $\Omega=\sqrt{\omega_0^2-\gamma^2/4}$. By using Eqs. (13), (15), and (9), the two-dimensional Raman scattering spectrum can be obtained.

Since the two difference frequencies, Ω_1 and Ω_2, have clear physical meanings, it is now possible to predict the outcomes for a few cases that are a bit more complicated than that of the single damped harmonic oscillator. Hereafter, we shall mainly focus on the E-E region, that is to say, both Ω_1 and Ω_2 are greater than zero, which is achieved by controlling the three field frequencies as $\omega_1\geqslant\omega_2$ and $\omega_1\geqslant\omega_3$.

B. Two harmonic oscillators: Uncoupled case

When we consider two vibrational modes, there are a few cases to be carefully investigated. In order to give a physical picture of coupling or mixing of two vibrational modes, we should distinguish two sources of couplings. The first arises from mode coupling in the vibrational potential energy. For instance, the normal mode analysis of a given system provides the uncoupled harmonic coordinates as the first-order approximation to the complicated multidimensional potential surface. Then one can express the potential as

$$V(\mathbf{Q})=V_0+\frac{1}{2}\sum_k m_k\omega_k^2Q_k^2+\frac{1}{6}\sum_k\sum_l\sum_m\left(\frac{\partial^3V}{\partial Q_k\partial Q_l\partial Q_m}\right)_n Q_kQ_lQ_m+\cdots, \tag{16}$$

where Q_k denotes the kth normal mode. If one truncates the potential at the second order, the system consists of a collection of uncoupled harmonic oscillators. On the other hand, the third term is responsible for the anharmonic coupling (AC) effects. This is the first source of mode coupling we shall discuss later. The second source is due to the polarizability coupling (PC), which is induced by the second-order derivative terms in the polarizability expansion with respect to the coordinates

$$\alpha(\mathbf{Q})=\alpha_0+\sum_k \left(\frac{\partial\alpha}{\partial Q_k}\right)Q_k+\frac{1}{2}\sum_{j,k}\left(\frac{\partial\alpha}{\partial Q_j\partial Q_k}\right)Q_jQ_k+\cdots . \tag{17}$$

If we assume that the off-diagonal components in the third term in Eq. (17), such as $(\partial\alpha/\partial Q_j\partial Q_k)$ for $j\neq k$, vanish, this means we assume that there are no PC terms. Having explained these two sources of mode coupling, we shall discuss the spectra in some limiting cases.

Suppose there are neither AC nor PC terms. That is to say, all vibrational modes are harmonic oscillators, also the polarizability expansions in Eq. (17) should be simply

$$\alpha(\mathbf{Q})=\alpha_0+\sum_k \left(\frac{\partial\alpha}{\partial Q_k}\right)Q_k+\frac{1}{2}\sum_{k}\left(\frac{\partial^2\alpha}{\partial Q_k^2}\right)Q_k^2+\cdots . \tag{18}$$

In this case the nonlinear Raman response function can have terms like

$$\langle[[Q_j^2(\tau_1+\tau_2),Q_j(\tau_1)],Q_j(0)]\rangle, \tag{19a}$$

$$\langle[[Q_k^2(\tau_1+\tau_2),Q_j(\tau_1)],Q_j(0)]\rangle \quad \text{for } j\neq k. \tag{19b}$$

The term like Eq. (19a) produces a series of single harmonic mode spectra having peaks along the diagonal in addition to those along the Ω_1 and Ω_1 axes, and do not produce any cross peaks. Interestingly the resonance peaks associated with terms like Eq. (19b) do not contribute to the spectrum in the E-E region either. In fact, the contributions from Eq. (19b) should appear as diagonal peaks in the E-D as well as D-E regions of the COTRAS spectrum. This can be understood from the energy level diagrams. At time $t=0$, the jth mode is excited and then at $t=\tau_1$ that mode should be deexcited, and at $t=\tau_1+\tau_2$ the kth mode is simultaneously excited and deexcited. Because the first two processes constitute the excitation and deexcitation of the jth harmonic mode, this contribution appears in E-D as well as D-E regions of the COTRAS spectrum. Therefore, *in this case of no-AC and no-PC terms, there is no cross peak at, for instance,* $\Omega_1=\omega_j$ *and* $\Omega_2=\omega_k$ *for* $j\neq k$. In other words, if the cross peaks at the off-diagonal region of the E-E COTRAS spectrum are found, this strongly indicates that there are either AC or PC or both. How strong these cross peaks are is therefore related to how large AC or PC effects are.

In order to confirm the above qualitative discussions on the COTRAS spectrum of uncoupled harmonic oscillators, we consider two harmonic oscillators without AC nor PC. In order to numerically calculate the spectrum, we used the Brownian oscillator model and summarized the expressions in the Appendix (for more detailed discussions on the model calculations, refer to Ref. 18(c)). In this case, the linear response function of each harmonic oscillator is given as Eq. (15). We first calculate the COTRAS spectrum for a single harmonic oscillator and it is shown in Fig. 4(a). Here the frequency of Q_1 mode, ω_1^0, is assumed to be 400 cm^{-1}, and the damping constant, γ_1, equals to 30 cm^{-1}. The three peaks at $(\Omega_1=\omega_1^0,\Omega_2=0)$, $(\Omega_1=0,\Omega_2=\omega_1^0)$, and $(\Omega_1=\omega_1^0,\Omega_2=\omega_1^0)$, that are denoted as 1, 2, and 3, appear in the E-E region. Also peaks 4 and 5, that are associated with a sequential excitation–deexcitation process, are observed in the E-D and D-E regions. The peak 6 can be interpreted as (i) two quanta excitation of the ω_1^0-mode at time $t=0$, (ii) one quantum deexcitation at $t=\tau_1$, and (iii) one quantum deexcitation at $t=\tau_1+\tau_2$. In case of two harmonic modes that are coupled via neither PC nor AC mechanisms, the COTRAS spectrum is plotted in Fig. 4(b). Here, the frequency of the Q_2 mode, ω_2^0, is assumed to be 600 cm^{-1}, and $\gamma_2=15$ cm^{-1}. As can be seen in Fig. 4(b), we find more peaks along the diagonal as well as along the two axes. However, one can easily interpret each peak in terms of excitation and deexcitation of corresponding vibrational modes as was discussed above for the case of a single vibrational mode.

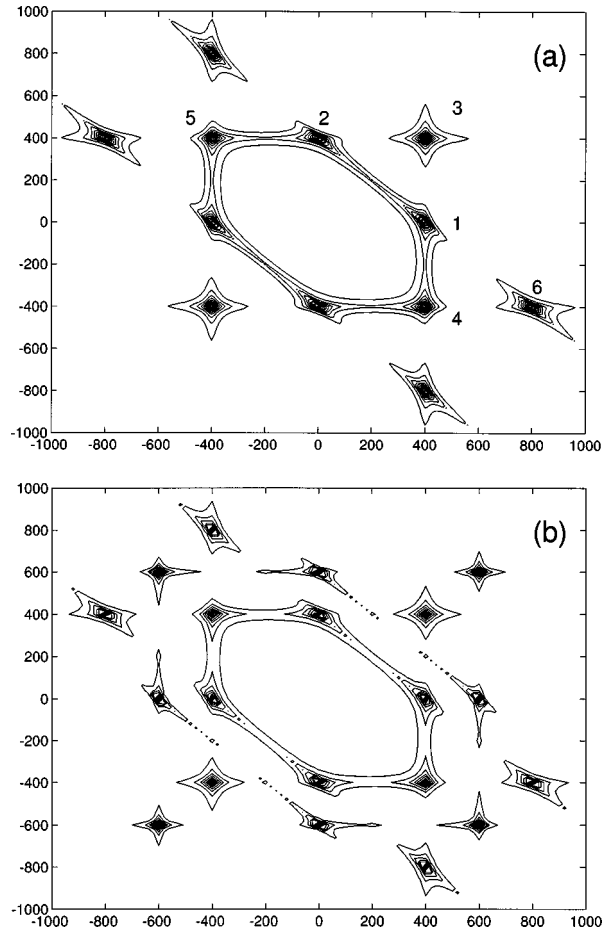

FIG. 4. (a) The square root of the COTRAS spectrum, $\{S_{\mathrm{COTRAS}}(\Omega_1,\Omega_2)\}^{1/2}=|\tilde{R}^{(5)}(\Omega_1,\Omega_1+\Omega_2)+\tilde{R}^{(5)}(\Omega_2,\Omega_1+\Omega_2)|$, of a single damped harmonic oscillator whose frequency ω_1^0 and damping constant γ_1 are 400 and 30 cm^{-1}. This spectrum is calculated by using Eq. (A4). (b) The square root of the COTRAS spectrum, $\{S_{\mathrm{COTRAS}}(\Omega_1,\Omega_2)\}^{1/2}$, of two uncoupled damped harmonic oscillators. The frequency ω_2^0 and damping constant γ_2 of the second (higher-frequency) mode are 600 and 15 cm^{-1}. Also the ratio of $(\alpha_1^{(1)})^2/M_1\zeta_1$ to $(\alpha_1^{(2)})^2/M_2\zeta_2$, that is $[(\alpha_1^{(1)})^2/M_1\zeta_1]/[(\alpha_1^{(2)})^2/M_2\zeta_2]$, is assumed to be 1/0.6. For the sake of convenience, the second-derivatives of the polarizability are assumed to be $\alpha_2^{(ss)}=(\alpha_1^{(s)})^2$. Since it is assumed that the off-diagonal second-derivatives of the polarizability, $\alpha_2^{(12)}=\alpha_2^{(21)}=\partial^2\alpha/\partial Q_1\partial Q_2$, are zero, the two modes are not coupled via PC nor AC.

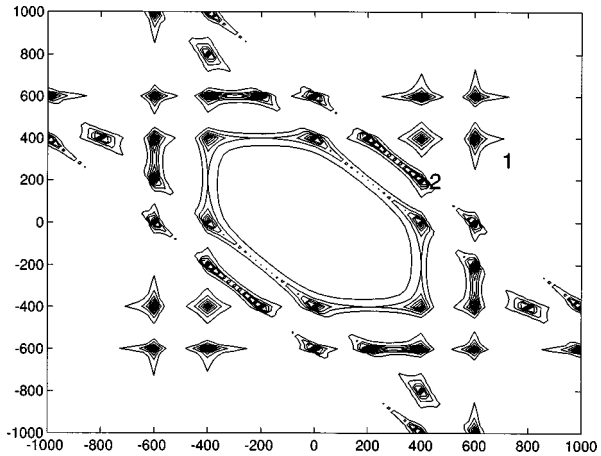

FIG. 5. The square root of the COTRAS spectrum, $\{S_{\mathrm{COTRAS}}(\Omega_1,\Omega_2)\}^{1/2}$, of two damped harmonic oscillator coupled via PC. In contrast to Fig. 4(b), the off-diagonal elements of the second derivatives of the polarizability, $\alpha_2^{(12)}=\alpha_2^{(21)}=\partial^2\alpha/\partial Q_1\partial Q_2$, are assumed to be $\alpha_2^{(12)}=\alpha_2^{(21)}=\alpha_1^{(1)}\alpha_1^{(2)}$.

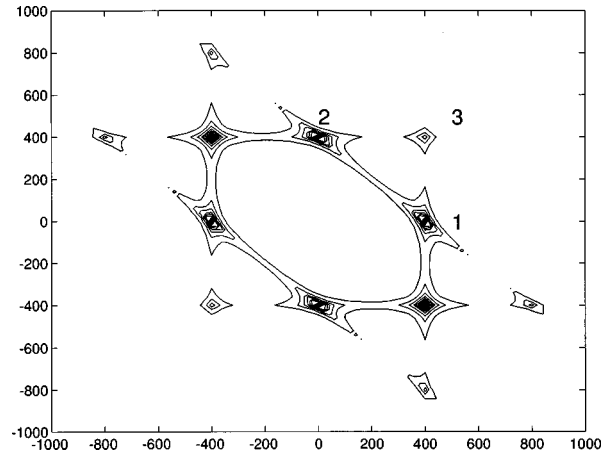

FIG. 6. The square root of the COTRAS spectrum of a single anharmonic oscillator with same frequency and damping constant in Fig. 4(a). It is assumed that $\partial^2\alpha/\partial Q^2=0$. This is calculated by using Eq. (A6).

C. Two harmonic oscillators: PC effects without AC

In Sec. III B, two types of mode couplings were introduced. In this section, two harmonic oscillators without any AC effects are considered. Then the PC effects should be the only source of mode coupling. In addition to the contributions associated with each individual harmonic oscillator to the COTRAS spectrum, there are more terms contributing to COTRAS process, that are, for $j\neq k$

$$\begin{aligned}&\langle[[Q_jQ_k(\tau_1+\tau_2),Q_k(\tau_1)],Q_j(0)]\rangle,\\&\langle[[Q_k(\tau_1+\tau_2),Q_jQ_k(\tau_1)],Q_j(0)]\rangle,\\&\langle[[Q_k(\tau_1+\tau_2),Q_j(\tau_1)],Q_jQ_k(0)]\rangle.\end{aligned}\tag{20}$$

These terms are proportional to $(\partial\alpha/\partial Q_j)(\partial\alpha/\partial Q_k)\times(\partial^2\alpha/\partial Q_j\partial Q_k)$. They contribute to the E-E region of the COTRAS spectrum. The first term in Eqs. (20), for instance, should be associated with the process, (i) one quantum excitation of the jth mode, (ii) one quantum excitation of the kth mode, and (iii) one quantum deexcitations of both the jth and kth modes. Consequently, two cross peaks at ($\Omega_1=\omega_j^0$ and $\Omega_2=\omega_k^0$) and ($\Omega_1=\omega_k^0$ and $\Omega_2=\omega_j^0$) should appear. Therefore, the existence of the cross peaks is a clear manifestation of the polarizability coupling, when the anharmonicities of vibrational modes are weak. In order to confirm this observation, we numerically calculate the spectrum of the two harmonic oscillators with PC and no AC, Fig. 5. In addition to the peaks appearing in Fig. 4(b), there clearly exist cross peaks and the intensity of these peaks strongly depends on the polarizability coupling constant, $(\partial^2\alpha/\partial Q_1\partial Q_2)$. For instance, peak 1 corresponds to the process given by the first term in Eq. (20), e.g., (i) excitation of Q_2 mode at $t=0$, (ii) excitation of Q_1 mode at $t=\tau_1$, and (iii) simultaneous deexcitations of both Q_1 and Q_2 modes at $t=\tau_1+\tau_2$. The peak 2 is produced by the process given by the second term in Eq. (20), (i) excitation of Q_1 mode at $t=0$, (ii) simultaneous deexcitation of Q_1 mode with excitation of Q_2 mode at $t=\tau_1$, and (iii) deexcitation of Q_2 mode at $t=\tau_1+\tau_2$. Therefore, during the second period, τ_2, the system evolves an oscillatory motion with frequency of $\omega_k^0-\omega_j^0$, which is 200^{-1} in the model calculation.

D. A single damped anharmonic oscillator

In case when the anharmonicity is present, the nonlinear Raman response function also contains a term like

$$\langle[[Q(\tau_1+\tau_2),Q(\tau_1)],Q(0)]\rangle.\tag{21}$$

Because of the anharmonicity, the trace given above does not vanish. The magnitude of this contribution is proportional to $(\partial\alpha/\partial Q)^3(\partial^3V/\partial Q^3)$. Equation (21) can be also interpreted as the three consecutive processes, i.e., (i) one quantum excitation from $n=0$ to $n=1$ at time $t=0$, (ii) one quantum excitation from $n=1$ to $n=2$ at $t=\tau_1$, and (iii) two quantum deexcitation from $n=2$ to 0 at $t=\tau_1+\tau_2$ [see Fig. 3(d)]. Then this process results in peaks around the diagonal line. Here, n is the vibrational quantum number. The third process, (iii), is allowed because of the anharmonicity. In this case the contribution from Eq. (21) may not produce a peak at exactly diagonal position because the frequency differences between $|n=0\rangle$ and $|n=1\rangle$ and between $|n=1\rangle$ and $|n=2\rangle$ are different. Consequently, the *split off-diagonal peaks* could appear at ($\Omega_1=\omega_{10}$ and $\Omega_2=\omega_{21}$) as well as ($\Omega_1=\omega_{21}$ and $\Omega_2=\omega_{10}$), where $\omega_{\beta,\alpha}\equiv(E_\beta-E_\alpha)/\hbar$. However it is possible that this splitting is so small that they cannot be clearly resolved in the case of weak anharmonicity as well as of large broadening.

In addition to the contributions from the anharmonic potential, the contributions associated with polarizability expansion term such as α_2Q^2 are to be included. Then the three kinds of terms in Eqs. (12) should be considered also. Since the two distinctive contributions, that are proportional to anharmonicity [Eq. (21)] and to the second derivative of the polarizability [Eqs. (12)], are additive, it is likely that the distinction of one over the other from the spectrum is difficult.

In Fig. 6, we present the COTRAS spectrum of a single

anharmonic oscillator with the cubic anharmonicity, i.e.,

$$V(Q)=\tfrac{1}{2}kQ^2+gQ^3,$$

where k is the force constant and g is the cubic anharmonic constant (see the Appendix for detailed expressions for the model calculations). Here, it is assumed that $\partial^2\alpha/\partial Q^2$ is negligibly small so that the spectrum is solely determined by the nonzero cubic anharmonicity. Now Fig. 6 should be compared with Fig. 4(a), where $g=0$ and $\partial^2\alpha/\partial Q^2\neq 0$. Both figures contain common peaks, but the relative intensities are different for each case. For example, the peak 3 along the diagonal line in Fig. 4(a) is as strong as the peak 1 on the Ω_1 axis. However, when the spectrum is governed by the anharmonicity, the diagonal peak 3 in Fig. 6 is much weaker than the peaks on the axes, peaks 1 and 2. Therefore, for a given mode, it may be possible to distinguish the two different cases by comparing the diagonal peaks and those on the axes, given that one can assume that one of the two processes, either the anharmonicity, g, or the second derivative of the polarizability, $\partial^2\alpha/\partial Q^2$, dominates.

E. Anharmonically coupled oscillators: Without quadratic terms in the polarizability expansion

In order to clarify the anharmonic coupling effects on the COTRAS spectrum, we assume that the vibrational potential energy of the two harmonic oscillators can be written as

$$\text{Case 1}: V(Q_1,Q_2)=\frac{1}{2}\sum_{j=1}^{2} m_j\omega_j^2Q_j^2+\frac{g_{211}}{2}Q_2Q_1^2, \tag{22a}$$

$$\text{Case 2}: V(Q_1,Q_2)=\frac{1}{2}\sum_{j=1}^{2} m_j\omega_j^2Q_j^2+\frac{g_{122}}{2}Q_1Q_2^2. \tag{22b}$$

These two cases contain cubic anharmonic coupling terms whose anharmonicities are represented by the constants, g_{211} and g_{122}. Furthermore, for the sake of clarity, we assume that there are no quadratic terms in the polarizability expansion, that is to say,

$$\alpha(Q_1,Q_2)=\alpha_0+\sum_{j=1}^{2}\left(\frac{\partial\alpha}{\partial Q_j}\right)Q_j.$$

Therefore, the usual diagonal peaks induced by the contributions such as $\langle[[Q_j^2(\tau_1+\tau_2),Q_j(\tau_1)],Q_j(0)]\rangle$ are ignored. Therefore, the peaks for this simplified case are to be purely related to the anharmonic coupling effects. Then, there are terms contributing to the signal such as

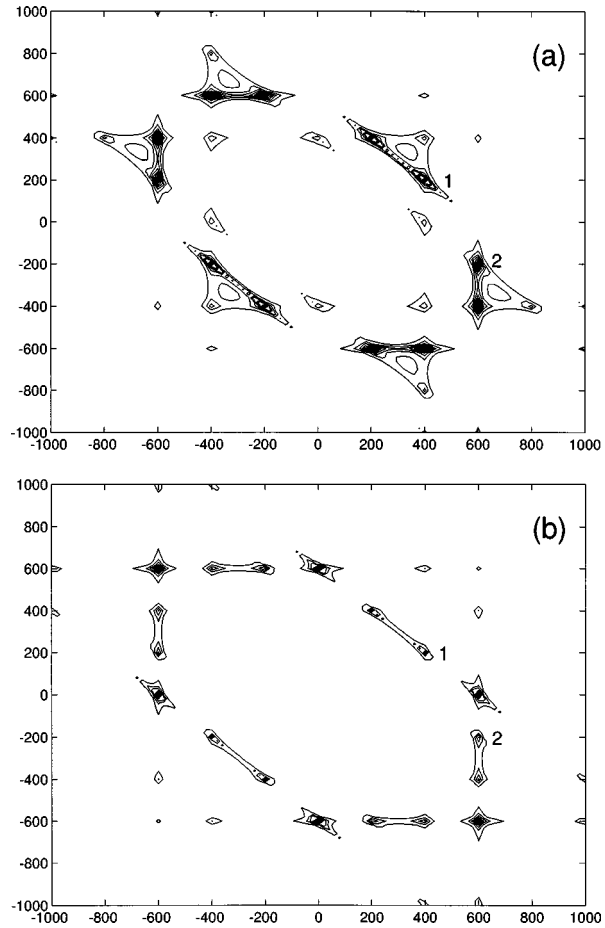

FIG. 7. (a) The square root of the COTRAS spectrum of two anharmonically coupled oscillators [Case 1 given in Eq. (22a)]. The frequencies and damping constants of the two oscillators are identical to those in Fig. 4(b). (b) The square root of the COTRAS spectrum of Case 2 given in Eq. (22b).

$$\begin{aligned}
&\langle[[Q_2(\tau_1+\tau_2),Q_1(\tau_1)],Q_1(0)]\rangle,\\
&\langle[[Q_1(\tau_1+\tau_2),Q_2(\tau_1)],Q_1(0)]\rangle,\\
&\langle[[Q_1(\tau_1+\tau_2),Q_1(\tau_1)],Q_2(0)]\rangle,\\
&\langle[[Q_1(\tau_1+\tau_2),Q_2(\tau_1)],Q_2(0)]\rangle,\\
&\langle[[Q_2(\tau_1+\tau_2),Q_1(\tau_1)],Q_2(0)]\rangle,\\
&\langle[[Q_2(\tau_1+\tau_2),Q_2(\tau_1)],Q_1(0)]\rangle.
\end{aligned} \tag{23}$$

In case 1, where there are cubic coupling term, $g_{211}Q_2Q_1^2$, the Q_1 mode becomes the dominant contribution to the 2D spectrum on the Ω_1 and Ω_2 axes as well as on the diagonal line [see Fig. 7(a)]. In other words, the peak intensities associated with Q_1 mode are stronger than any other ones. Once again we emphasize that, because it was assumed that there are no second-derivative terms in the polarizability expansion, the spectral features appearing in Fig. 7(a) purely originate from the anharmonic coupling. In case 2, where the anharmonic coupling term is dominated by $g_{122}Q_1Q_2^2$, the Q_2-mode contributions to the spectrum on the Ω_1 and Ω_2 axes as well as on the diagonal line are dominant features, as can be seen in Fig. 7(b). Furthermore, the combination peaks 1 and 2 in Fig. 7 are very strong in both cases 1 and 2.

Therefore, by carefully examining these regions of the spectrum one can obtain some qualitative information on the anharmonic mode coupling.

IV. SUMMARY AND A FEW CONCLUDING REMARKS

The main purpose of this paper was to propose a new frequency-domain experiment measuring the coherent two-dimensional Raman scattering process. By using three fields with different wave vectors and frequencies and measuring the signal with $\mathbf{k}_s = 3\mathbf{k}_1 - \mathbf{k}_2 - \mathbf{k}_3$ and $\omega_s = 3\omega_1 - \omega_2 - \omega_3$, the off-resonant two-dimensional Raman scattering spectrum can be obtained in terms of the nonlinear Raman response function. Thereby one can make a direct comparison with the time-domain femtosecond 2D Raman spectroscopy investigated recently. We found that the COTRAS spectrum is diagonally symmetric. By comparing the frequency-domain spectrum with that obtained from the femtosecond time-domain measurement, it may be possible to study the slowly varying and almost static inhomogeneous distribution of vibrational modes. Suppose that the vibrational frequencies are inhomogeneously distributed and the distribution is slowly changing in time so that the distribution function can be approximated as $S(\Gamma, T)$, where Γ represents the set of vibrational mode parameters, such as the frequency and strength of interaction. Then the fifth-order response function should be given by the average over this distribution function as

$$R^{(5)}(\tau_1, \tau_2) = \int d\Gamma \; S(\Gamma, T = \tau_1 + \tau_2) R^{(5)}(\tau_1, \tau_2; \Gamma). \tag{24}$$

The time-domain experiment can measure the inhomogeneity for a fixed T, whereas the frequency-domain one measures the time-averaged quantity given by Eqs. (7) and (24). Therefore, if one finds a difference between the time-domain spectrum and that obtained from the frequency-domain measurement, this is likely to be an evidence of the slowly varying time-dependent inhomogeneous distribution.

In case of an harmonic oscillator, three peaks in the excitation–excitation frequency domain of the COTRAS spectrum are to be found, where the diagonal peak represents the consecutive two quanta excitations so that two vibrational coherent states are related to this process. When anharmonicity is present, the difference frequencies between the ground and first excited states and between the first and second excited states are different. As a result, one could find a pair of splitted peaks around the diagonal axis, depending on the anharmonicity as well as the spectral broadening. In case of polarizability coupling [see Eq. (17) and discussions below Eq. (17)], the cross peaks appear even for two harmonic oscillators. The intensity of these peaks is proportional to the second derivative of the polarizability with respect to the two vibrational coordinates. Also if there is an anharmonic coupling between two modes, the cross peaks show up in the spectrum. From the numerical analysis, it was found that the relative intensities of the diagonal peaks compared to the peaks along the axes are small when the anharmonicities are the dominant mechanism for fifth-order Raman response. However, if both polarizability coupling and anharmonic mode coupling contribute to the spectrum, it is difficult to distinguish the relative importance of each contribution without extensive numerical calculations. Therefore it is desired to carry out a more detailed investigation by molecular dynamics simulation and quantum chemistry calculations. Also it will be very interesting to conduct the COTRAS experiment in the gas phase to get a detailed information on the mode couplings among the intramolecular vibrational modes as discussed in this paper.

ACKNOWLEDGMENTS

M.C. is grateful for the supports from KOSEF, MOST/STEPI, and Center for Molecular Science. This work was partly supported by the Japan–Korea collaboration program. M.C. is also very grateful for the hospitality of researchers in the theoretical division of the Institute for Molecular Science during his stay. We thank Dr. Andrei Tokmakoff for very helpful discussions.

APPENDIX

In this appendix we present the analytic expressions for the fifth-order Raman response functions associated with the polarizability- and anharmonic-coupling processes, that are denoted as R_P and R_A, respectively. See Ref. 18(c) for detailed derivation of these results, where the Feynman rule on the unified path was used.[18(a),18(b),22] The total response function is given by a sum of the two contributions, $R = R_P + R_A$. By defining $\alpha_1^{(j)}$ and $\alpha_2^{(jk)}$ as

$$\alpha_1^{(j)} \equiv \frac{\partial \alpha}{\partial Q_j}, \qquad \alpha_2^{(jk)} \equiv \frac{\partial^2 \alpha}{\partial Q_j \partial Q_k}, \tag{A1}$$

we find that the two response functions are

$$\begin{aligned} R_P &= -\frac{1}{\hbar^2} \sum_{jk} \alpha_1^{(j)} \alpha_1^{(k)} \alpha_2^{(jk)} G_j(\tau_2) [G_k(\tau_1 + \tau_2) \\ &\quad + G_k(\tau_1)], \\ R_A &= \frac{i}{\hbar^3} \sum_{jkl} g_{jkl} \alpha_1^{(j)} \alpha_1^{(k)} \alpha_1^{(l)} \int_0^\infty dt G_j(\tau_1 + \tau_2 - t) \\ &\quad \times G_k(t) G_l(t - \tau_1), \end{aligned} \tag{A2}$$

where the linear response function is

$$G_j(t) \equiv \theta(t) \frac{\hbar}{i M_j \zeta_j} \exp(-\gamma_j t/2) \sin \zeta_j t. \tag{A3}$$

Here, $\theta(t)$ is a heavy-side step function and $\zeta_j \equiv \sqrt{(\omega_j^0)^2 - \gamma_j^2/4}$. ω_j^0 and γ_j are the frequency and damping constant of the jth mode. g_{jkl} is the corresponding cubic

anharmonic constant. From these results, the Fourier–Laplace transform of the polarizability coupled contribution is found to be

$$\widetilde{R}_P(\omega_\alpha,\omega_\beta)=\frac{1}{2}\sum_{jk}\frac{\alpha_1^{(j)}\alpha_1^{(k)}\alpha_2^{(jk)}}{M_jM_k\zeta_j\zeta_k}\sum_{n=1}^{4}(-1)^n\frac{-\Omega_{1n}\Omega_{2n}+\Gamma\Gamma_n-i\Gamma_n\omega_\alpha-i\Gamma\omega_\beta-\omega_\alpha\omega_\beta}{(\Gamma^2+\Omega_{1n}^2-2i\Gamma\omega_\alpha-\omega_\alpha^2)(\Gamma_n^2+\Omega_{2n}^2-2i\Gamma_n\omega_\beta-\omega_\beta^2)},\tag{A4}$$

where

$$\Gamma\equiv\gamma_k/2,$$

$$\begin{pmatrix}\Gamma_1 & \Omega_{11} & \Omega_{21}\\ \Gamma_2 & \Omega_{12} & \Omega_{22}\\ \Gamma_3 & \Omega_{13} & \Omega_{23}\\ \Gamma_4 & \Omega_{14} & \Omega_{24}\end{pmatrix}\equiv\begin{pmatrix}\gamma_j/2 & \zeta_k & \zeta_j\\ \gamma_j/2 & -\zeta_k & \zeta_j\\ (\gamma_j+\gamma_k)/2 & \zeta_k & \zeta_j+\zeta_k\\ (\gamma_j+\gamma_k)/2 & -\zeta_k & \zeta_j-\zeta_k\end{pmatrix}.\tag{A5}$$

The Fourier–Laplace transform of the anharmonicity-coupled contribution to the response function is

$$\widetilde{R}_A(\omega_\alpha,\omega_\beta)=-\sum_{jkl}g_{jkl}\frac{\alpha_1^{(j)}\alpha_1^{(k)}\alpha_1^{(l)}}{4M_jM_kM_l\zeta_j\zeta_k\zeta_l}\sum_{n=1}^{4}(-1)^n(\widetilde{F}_{1n}-\widetilde{F}_{2n})\tag{A6}$$

with

$$\widetilde{F}_{mn}\equiv\frac{\Gamma_0[\Omega_{2n}^{(m)}(\Gamma-i\omega_\alpha)+\Omega_{1n}(\Gamma_m-i\omega_\beta)]+\Omega_{0n}(-\Omega_{1n}\Omega_{2n}^{(m)}+\Gamma\Gamma_m-i\Gamma_m\omega_\alpha-i\Gamma\omega_\beta-\omega_\alpha\omega_\beta)}{(\Gamma_0^2+\Omega_{0n}^2)(\Gamma^2+\Omega_{1n}^2-2i\Gamma\omega_\alpha-\omega_\alpha^2)(\Gamma_m^2+(\Omega_{2n}^{(m)})^2-2i\Gamma_m\omega_\beta-\omega_\beta^2)}.\tag{A7}$$

Here, the coefficients are defined as

$$\begin{pmatrix}\Gamma_0 & \Gamma & \Gamma_1 & \Gamma_2\\ \Omega_{01} & \Omega_{11} & \Omega_{21}^{(1)} & \Omega_{21}^{(2)}\\ \Omega_{02} & \Omega_{12} & \Omega_{22}^{(1)} & \Omega_{22}^{(2)}\\ \Omega_{03} & \Omega_{13} & \Omega_{23}^{(1)} & \Omega_{23}^{(2)}\\ \Omega_{04} & \Omega_{14} & \Omega_{24}^{(1)} & \Omega_{24}^{(2)}\end{pmatrix}$$

$$\equiv\begin{pmatrix}(-\gamma_j+\gamma_k+\gamma_l)/2 & \gamma_k/2 & (\gamma_k+\gamma_l)/2 & \gamma_j/2\\ -\zeta_j-\zeta_k+\zeta_l & -\zeta_k & -\zeta_k+\zeta_l & \zeta_j\\ -\zeta_j+\zeta_k+\zeta_l & \zeta_k & \zeta_k+\zeta_l & \zeta_j\\ -\zeta_j+\zeta_k-\zeta_l & \zeta_k & \zeta_k-\zeta_l & \zeta_j\\ -\zeta_j-\zeta_k-\zeta_l & -\zeta_k & -\zeta_k-\zeta_l & \zeta_j\end{pmatrix}.\tag{A8}$$

The corresponding response function for COTRAS is

$$R_{\mathrm{COTRAS}}=\widetilde{R}(\Omega_1,\Omega_1+\Omega_2)+\widetilde{R}(\Omega_2,\Omega_1+\Omega_2),$$

where $\widetilde{R}(\omega_1,\omega_2)=\widetilde{R}_P(\omega_1,\omega_2)+\widetilde{R}_A(\omega_1,\omega_2)$. We used Eqs. (A4) and (A6) to numerically calculate the COTRAS spectra shown in Figs. 4, 5, 6, and 7.

[1] N. Bloembergen, *Nonlinear Optics* (Benjamin, New York, 1965).
[2] Y. R. Shen, *The Principles of Nonlinear Optics* (Wiley, New York, 1984).
[3] S. Mukamel, *Principles of Nonlinear Optical Spectroscopy* (Oxford University Press, New York, 1995).
[4] D. McMorrow, W. T. Lotshaw, and G. A. Kenney-Wallace, IEEE J. Quantum Electron. **QE-24**, 443 (1988); D. McMorrow and W. T. Lotshaw, J. Phys. Chem. **95**, 10395 (1991).
[5] T. Hattori and T. Kobayashi, J. Chem. Phys. **94**, 3332 (1991).
[6] M. Cho, M. Du, N. F. Scherer, G. R. Fleming, and S. Mukamel, J. Chem. Phys. **99**, 2410 (1993).
[7] S. Palese, J. T. Buontempo, L. Schilling, W. T. Lotshaw, Y. Tanimura, S. Mukamel, and R. J. D. Miller, J. Phys. Chem. **98**, 12466 (1994).
[8] Y. J. Chang and E. W. Castner, Jr., J. Chem. Phys. **99**, 113, 7289 (1993).
[9] H. P. Duel, P. Cong, and J. D. Simon, J. Phys. Chem. **98**, 12600 (1994).
[10] S. Ruhman, A. G. Joly, and K. A. Nelson, J. Chem. Phys. **86**, 6563 (1987); S. Ruhman, A. G. Joly, and K. A. Nelson, IEEE J. Quantum Electron. **QE-24**, 460 (1988); Y. X. Yan and K. A. Nelson, J. Chem. Phys. **87**, 6240,6257 (1987); Y. J. Chang, P. Cong, and J. D. Simon, J. Phys. Chem. **99**, 7857 (1995).
[11] P. Vohringer and N. S. Scherer, J. Phys. Chem. **99**, 2684 (1995).
[12] G. R. Fleming and M. Cho, Annu. Rev. Phys. Chem. **47**, 109 (1996).
[13] M. Cho and G. R. Fleming, Adv. Chem. Phys. (in press, 1998).
[14] Y. Tanimura and S. Mukamel, J. Chem. Phys. **99**, 9496 (1993); K. Okumura and Y. Tanimura, J. Chem. Phys. **106**, 1687 (1997).
[15] K. Tominaga and K. Yoshihara, Phys. Rev. Lett. **74**, 3061 (1995); K. Tominaga, G. P. Keogh, Y. Naitoh, and K. Yoshihara, J. Raman Spectrosc. **26**, 495 (1995); K. Tominaga and K. Yoshihara, J. Chem. Phys. **104**, 1159,4419 (1996).
[16] (a) A. Tokmakoff and G. R. Fleming, J. Chem. Phys. **106**, 2569 (1997); (b) A. Tokmakoff, M. J. Lang, D. S. Larsen, and G. R. Fleming, Chem. Phys. Lett. (in press); (c) A. Tokmakoff, M. J. Lang, D. S. Larsen, G. R. Fleming, V. Chernyak, and S. Mukamel, Phys. Rev. Lett. (submitted, 1997).
[17] (a) T. Steffen and K. Duppen, Phys. Rev. Lett. **76**, 1224 (1996); (b) T. Steffen and K. Duppen, J. Chem. Phys. **106**, 3854 (1997).
[18] (a) K. Okumura, and Y. Tanimura, J. Chem. Phys. **107**, 2267 (1997); (b) K. Okumura and Y. Tanimura, Chem. Phys. Lett. **277**, 159 (1997); (c) K. Okumura and Y. Tanimura, Chem. Phys. Lett. **278**, 175 (1997).
[19] S. Saito and I. Ohmine, J. Chem. Phys. (submitted, 1997).
[20] D. P. Craig and T. Thirunamachandran, *Molecular Quantum Electrodynamics, An Introduction to Quantum Electrodynamics* (Academic, London, 1984).
[21] T. Keyes and B. M. Ladanyi, Adv. Chem. Phys. **56**, 411 (1984).
[22] K. Okumura and Y. Tanimura, Phys. Rev. E **53**, 214 (1996); J. Chem. Phys. **105**, 7294 (1996); J. Chem. Phys. **106**, 1687 (1997); Phys. Rev. E **56**, 2747 (1997).